Organic–Inorganic Hybrid

DOI: 10.1002/anie.200804805

A Thermally and Hydrolytically Stable Microporous Framework Exhibiting Single-Chain Magnetism: Structure and Properties of $[Co_2(H_{0.67}bdt)_3]\cdot 20\,H_2O$**

Wayne Ouellette, Andrey V. Prosvirin, Kelly Whitenack, Kim R. Dunbar, and Jon Zubieta**

The widespread contemporary interest in hybrid organic–inorganic materials reflects fundamental interest in their compositional range and structural versatility, as well as applications to ion exchange, gas sorption, and catalysis.[1–6] The structural complexity of these materials, derived from the molecular-scale composite of inorganic and organic components, provides the potential for the design of novel multifunctional materials.[7,8]

The complex architectures of organic–inorganic hybrids are derived from metal, metal cluster, or metal oxide building blocks acting as nodes from which rigid or flexible multitopic organic ligands radiate to tether to adjacent nodes. The most common organic tethers are multitopic carboxylate and pyridine ligands.[9–11] Other ligand types, however, may be exploited to afford variable tether lengths, different charge-balance requirements, and juxtapositions of donor groups. The polyazaheteroaromatic ligands of the imidazole, pyrazole, triazole, and tetrazole types are quite attractive in view of their extensively documented ability to bridge metal ions to afford polynuclear compounds, their superexchange capacities reflected in unusual magnetic properties, and the facility of derivatization to provide additional functionality.[12–14] More recently, polyazaheteroaromatic ligands have been exploited in the design of microporous metal–organic frameworks with significant hydrogen-storage properties.[15,16] Furthermore, this class of ligands may be tethered and extended to mimic the linear dicarboxylates to provide spatial extension in the construction of frameworks with significant free volume. One example is 5,5′-(1,4-phenylene)bis(1*H*-tetrazole) (H_2bdt),[17] the manganese(II) compounds of which, such as $[Mn_3(bdt)_3(dmf)_4(H_2O)_2]\cdot$solvent, exhibit unusually effective hydrogen storage.

As part of our investigations of the structural diversity and the magnetic and luminescent properties of metal polyazaheteroaromatic frameworks,[18–22] we have prepared a hydrolytically and thermally stable microporous material $[Co_2(H_{0.67}bdt)_3]\cdot 20\,H_2O$ (**1**·20 H_2O). In addition to its microporous properties in the dehydrated state, **1**·20 H_2O exhibits single-chain magnetism and reversible changes in magnetism upon desolvation and resolvation.

The hydrothermal reaction of $CoSO_4\cdot 7\,H_2O$, H_2bdt, HF, and H_2O in the molar ratio 1.73:1.00:6.21:1190 at 180 °C for 48 h produced orange rods of **1**·20 H_2O in 80 % yield. The deprotonation of H_2bdt upon coordination to metal ions in the absence of strong bases is not uncommon.[16] The hydrothermal approach provides materials that are both hydrolytically and thermally robust.[23]

As shown in Figure 1, the structure of **1**·20 H_2O consists of a 3D metal–organic framework encompassing a considerable solvent-accessible volume.[24] The structure is constructed from $\{Co(tetrazolate)\}_n$ chains running parallel to the crystallographic *a* axis and linked through the phenyl tethers of the bdt ligands into a three-dimensional framework. Within the chains, each cobalt(II) site exhibits octahedral $\{CoN_6\}$

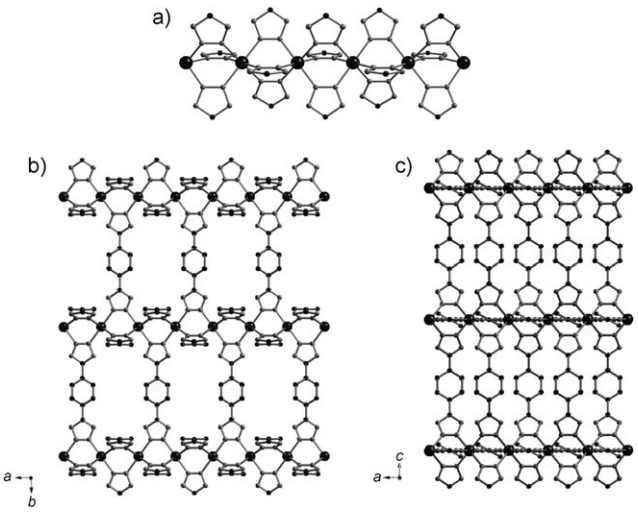

Figure 1. a) Ball-and-stick representation of the $\{Co(tetrazolate)\}_n$ chain substructure of **1**·20 H_2O, showing the exclusively six-coordinate cobalt sites. b, c) Views of the linking of chains through the phenyl tether of the bdt ligand in the *ab* plane (b) and the *ac* plane (c). In (b), the perspective masks two of the Co–N bonds, making the cobalt sites appear four-coordinate.

[*] Dr. W. Ouellette, K. Whitenack, Prof. J. Zubieta
Department of Chemistry
Syracuse University, Syracuse, NY 13244 (USA)
Fax: (+1) 315-443-4070
E-mail: jazubiet@syr.edu
Dr. A. V. Prosvirin, Prof. K. R. Dunbar
Department of Chemistry
Texas A&M University, College Station, TX 77842 (USA)
E-mail: dunbar@mail.chem.tamu.edu

[**] This work was supported by a grant from the National Science Foundation, CHE-0604527. K.W. acknowledges support from the NSF-REU program, CHE-0552753. The Micromeritics ASAP 2020 volumetric gas adsorption instrument was purchased with funds provided by Sam Nappi of Alliance Energy. H_2bdt = 5,5′-(1,4-phenylene)bis(1*H*-tetrazole).

Supporting information for this article is available on the WWW under http://dx.doi.org/10.1002/anie.200804805.

coordination through bonding to nitrogen donors of six bdt ligands. The chain connectivity is provided by bridging through the N2 and N3 sites of one tetrazolate terminus. A given chain is linked to four adjacent chains to provide three-dimensional connectivity and to generate the rectangular cavities parallel to the *a* axis. The chain substructure exhibits a three-bladed paddlewheel motif between metal sites, previously described for $[Fe(Htrz)_3](BF_4)_2{\cdot}H_2O$ and $[Mn_4(bdt)_3(NO_3)_2(def)_6]$ (Htrz = triazole, def = diethylformamide).[16,25] Charge compensation requires that 2/3 of the btd ligands remain singly protonated in the Hbdt form at the N2 or N4 site (Supporting Information, Figure S1). While the crystallography did not reveal the protonation site owing to symmetry and occupational considerations, the final electron density maps, as well as IR spectroscopy and elemental analysis, confirmed the absence of other potential charge-compensating groups. The connectivity pattern generates channels of approximate dimensions 12.0×9.0 Å, corresponding to 47.1% of the unit cell volume, which are occupied by H_2O molecules of crystallization.

Compound $\mathbf{1}{\cdot}20\,H_2O$ was analyzed by thermogravimetric analysis (TGA) under 20 mL min^{-1} flowing nitrogen while the temperature was raised at a rate of 5 °C min^{-1} from 25 to 800 °C. The thermal decomposition profile of $\mathbf{1}{\cdot}20\,H_2O$ exhibited a weight loss of approximately 28% between room temperature and 130 °C attributed to the loss of water of crystallization (32.3% theoretical). This process is followed by a plateau of stability between 130 and 290 °C, whereupon two discrete decomposition steps between 290 and 480 °C and a gradual weight loss to 800 °C result in an amorphous gray powder (Supporting Information, Figure S2). The thermodiffraction pattern for $\mathbf{1}{\cdot}20\,H_2O$ in the 24–450 °C range is largely unchanged to 325 °C, indicating that the Co bdt framework is thermally robust, persistent to 325 °C, and retained upon loss of water of crystallization (Supporting Information, Figure S3). Powder XRD of the hydrated $\mathbf{1}{\cdot}20\,H_2O$, the dehydrated **1**, and the rehydrated $\mathbf{1}{\cdot}x\,H_2O$ ($x \approx 19$) indicated that there was no significant structural change upon dehydration and rehydration, although there is some loss of crystallinity (Supporting Information, Figure S4).

Compound $\mathbf{1}{\cdot}20\,H_2O$ was desolvated under dynamic vacuum at 120 °C until the outgas rate was less than 2 mTorr min^{-1}. The desolvated host showed N_2 uptake of approximately 190 mL g^{-1} when $P > 0.05$ mm of Hg at 77.4 K and type I absorption behavior according to the IUPAC classification (Figure 2). The Brunauer–Emmett–Teller (BET) surface area was calculated from a line regression plot of $1/(W(P_0/P)-1)$ versus P_0/P, where W is the total volume absorbed at a particular point P_0/P and P_0 is 1 atm pressure, within the range $0.02 < P_0/P < 0.20$. The BET surface area is 729 m^2 g^{-1}, compared to a Langmuir surface area of 833 m^2 g^{-1}, which corresponds to an accessible void volume of 48%, in good agreement with the volume of 47% determined by X-ray crystallography (PLATON). The desolvated framework also exhibits considerable H_2 uptake with type I absorption behavior (Supporting Information, Figure S5). The uptake is 1.49% by weight at 120 kPa.

To prevent the loss of interstitial solvent, magnetic susceptibility measurements of $\mathbf{1}{\cdot}20\,H_2O$ were performed in a sealed plastic bag. Measurements were performed at 1000 Oe from 1.8 to 300 K with the use of a SQUID magnetometer. At 300 K, the product of molar susceptibility and temperature χT is 3.7 emu mol^{-1} K, which is higher than the value for a spin-only case ($\chi_{Co}T = 1.875$ emu mol^{-1} K, $S = 3/2$), as expected for an orbital contribution. As the temperature is lowered, the χT value decreases smoothly, which is attributed to spin–orbit coupling effects and possible antiferromagnetic interactions (Figure 3). The data were fit to the

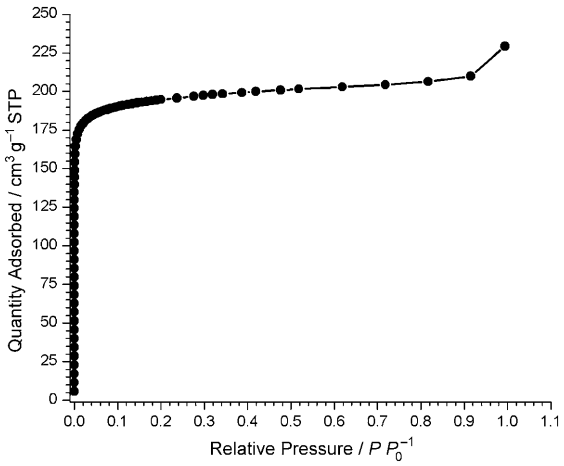

Figure 2. BET N_2 sorption isotherm for **1** at 77.4 K.

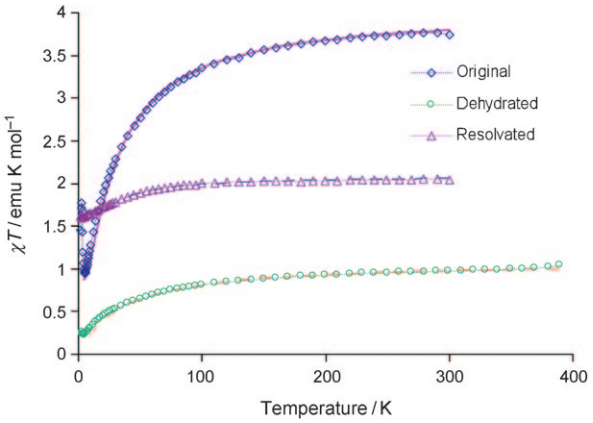

Figure 3. Temperature dependence of the χT product for $\mathbf{1}{\cdot}20\,H_2O$ (◇), **1** (○), and resolvated **1** (△). The solid line is the best fit to a Heisenberg chain model,[26] while the dashed lines are the best fits to the Curie–Weiss law.

Curie–Weiss law with parameters $\theta = -24$ K and $C = 4.1$ emu mol^{-1} K. Below 5 K, χT increases abruptly to reach a maximum at approximately 2 K and finally decreases again at lower temperatures. The data above 50 K were fit to the Fisher model for a one-dimensional chain with the Hamiltonian $H = -2J S_i S_{i-1}$, where J is the intrachain coupling constant, and S_i and S_{i-1} refer to spin operators of odd and even sites, respectively. The best fit was found for values of $J = -2.55$ cm^{-1} and $g = 2.9$.[26]

The polycrystalline sample was then filtered and dried in vacuo for 4 h. The magnetic behavior of this dry sample **1** was

found to be remarkably different from that of **1**·20 H_2O. The room-temperature value of χT is 1 emu mol^{-1} K, which indicates that more than 80% of the cobalt ions are now in a low-spin state ($\chi_{Co}T = 0.375$ emu mol^{-1} K, S = $^1/_2$). When the temperature is decreased, the χT value gradually decreases to a minimum at 2 K (Figure 3), an indication of antiferromagnetic interactions. The data were fit to the Curie–Weiss law with $\theta = -34$ K and $C = 1.09$ emu mol^{-1} K.

To gain more insight into the magnetic properties of **1**·20 H_2O, zero-field alternating-current (AC) susceptibility measurements were performed in the range of frequencies from 1 to 1000 Hz at $H_{AC} = 5$ Oe. The susceptibility shows a broad frequency-dependent out-of-phase signal below 5 K (Figure 4). The Mydosh parameter estimated from this

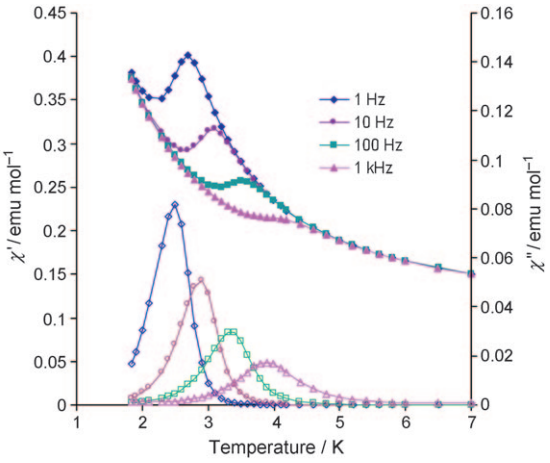

Figure 4. Temperature dependences of the real χ' (filled symbols) and imaginary χ'' components (open symbols) of the AC magnetic susceptibility of **1**·20 H_2O measured in an oscillating field of 5 Oe at different frequencies.

dependence, $\phi = (\Delta T_m/T_g)/\Delta\log\omega = 0.14$, ($\Delta T_m$ is the shift of the peak in χ'_m, ω is the applied frequency, and T_g is the position of the peak at zero frequency) is characteristic of normal superparamagnets and precludes the possibility of a spin-glass phase. The frequency dependence of the position of the peak in χ''_m follows an Arrhenius law (Figure 5, inset, and Supporting Information, Figure S6) with an activation energy

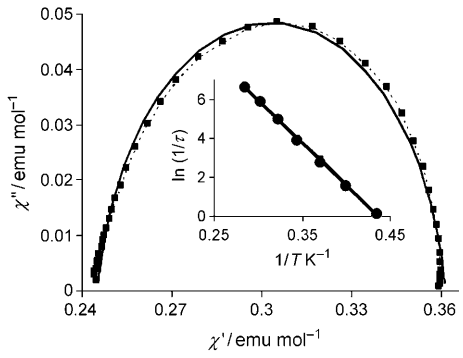

Figure 5. Cole–Cole diagram at 3 K. The solid line is the best fit to a generalized Debye model and the dashed line is a guide for the eyes. Inset: Arrhenius plot for **1**·20 H_2O.

$\Delta E/k_B = 30.2$ cm^{-1} (43.4 K) and $\tau_0 = 5.1\cdot10^{-9}$ s (k_B is the Boltzmann constant and τ_0 is a pre-exponential factor). The Cole–Cole plot (Figure 5)[27] exhibits a semicircular shape characteristic of a single relaxation process, confirming single-chain magnet behavior. It was fit to a generalized Debye model with an α value of 0.1, which indicates a narrow distribution of relaxation times. These parameters are similar to previously reported Co^{II} single-chain magnets and correlate well with the linear chain motif of **1**·20 H_2O.[28–33] Although the two cobalt centers in the chain are in identical environments of six nitrogen atoms, the corresponding ligand octahedra are rotated with respect to each other. The tilting of the anisotropy axes of the neighboring cobalt ions gives rise to an uncompensated magnetic moment. To confirm the single-chain magnet properties of **1**·20 H_2O, the hysteresis was measured at 1.8 K with a coercive field of 450 Oe (Supporting Information, Figure S7).

The dry sample no longer showed an out-of-phase AC signal. The magnetic susceptibility data indicate that after resolvation, the high-spin state is restored for approximately 50% of the cobalt(II) centers (Figure 3). However, the single-chain magnetic properties of the compound could not be restored owing to irreversible damage to the crystals (Supporting Information, Figure S8). Reversible changes in magnetic properties upon desolvation and resolvation of coordination frameworks have been observed in several cases, and the name "magnetic sponges" has been coined for such materials.[34–38]

In summary, hydrothermal chemistry has been exploited for the preparation of an open-framework thermally and hydrolytically stable material $[Co_2(H_{0.67}\cdot btd)_3]\cdot 20\,H_2O$ (**1**·20 H_2O). Upon desolvation, **1** exhibits type I isotherms, consistent with microporous character, and was shown to be capable of 1.49% hydrogen sorption by weight at 120 kPa. The compound also exhibited single-chain magnetic properties and reversible changes upon desolvation and resolvation.

Experimental Section

All chemicals were used as obtained without further purification: cobalt(II) sulfate heptahydrate and hydrofluoric acid (48 to 51%) were purchased from Aldrich. The ligand 5,5′-(1,4-phenylene)bis(1*H*-tetrazole) was prepared according to literature methods.[39] All syntheses were carried out in 23 mL poly(tetrafluoroethylene)-lined stainless steel containers under autogenous pressure. The reactants were stirred briefly, and the initial pH value was measured before heating. Water was distilled above 3.0 MΩ in-house using a Barnstead Model 525 Biopure Distilled Water Center. The initial and final pH value of the reaction were measured using Hydrion pH sticks.

1·20 H_2O: A solution of $CoSO_4\cdot 7H_2O$ (0.227 g, 0.808 mmol), 5,5′-(1,4-phenylene)bis(1*H*-tetrazole) (0.100 g, 0.467 mmol), H_2O (10.00 g, 556 mmol), and HF (48–51% HF, 0.100 mL, 2.898 mmol) was heated at 180 °C for 48 h (initial and final pH 2.2 and 2.0, respectively). The reaction vessel was removed from the oven and allowed to cool to room temperature under ambient conditions. Orange rods of **1**·20 H_2O suitable for X-ray crystallography were isolated in 80% yield. IR (KBr pellet): $\tilde{\nu}$ = 3404(b), 3077(w), 2889(w), 1693(m), 1558(m), 1437(s), 1273(m), 1236(w), 1191(w), 1162(m), 1069(s), 1003(m), 851(m), 768(w), 739(m), 552 cm^{-1}(s).

Structural measurements were performed on a Bruker-AXS SMART-CCD diffractometer at low temperature (90 K) using

graphite-monochromated $Mo_{K\alpha}$ radiation (0.71073 Å). The data were corrected for Lorentz and polarization effects and absorption using SADABS. The structure was solved by direct methods. All non-hydrogen atoms were refined anisotropically. After all of the non-hydrogen atoms were located, the model was refined against F^2, initially using isotropic and later anisotropic thermal displacement parameters. Hydrogen atoms were introduced in calculated positions and refined isotropically. Neutral atom scattering coefficients and anomalous dispersion corrections were taken from the literature.[40a] All calculations were performed using SHELXTL crystallographic software packages.[40a] The contribution of the solvent to the diffraction pattern in $[Co_2(bdt)(Hbdt)_2]\cdot 20H_2O$ ($\mathbf{1}\cdot 20H_2O$) was subtracted from the observed data by the SQUEEZE method implemented in PLATON.[40c,41] Crystal data for $\mathbf{1}\cdot 20H_2O$: $C_3H_{6.5}Co_{0.25}N_3O_{2.5}$, orthorhombic, *Cmmm*, $M_r = 139.34$, $a = 7.5320(6)$, $b = 26.296(2)$, $c = 12.522(1)$ Å, $V = 2480.1(3)$ Å^3, $Z = 16$, $\rho_{calcd} = 1.493\ g\,cm^{-1}$, $\mu = 0.762\ mm^{-1}$, $F(000) = 1156$, $R1 = 0.0400$, $wR2 = 0.0901$ (all data, 1781 reflections). CCDC 697453 contains the supplementary crystallographic data for this paper. These data can be obtained free of charge from The Cambridge Crystallographic Data Centre via www.ccdc.cam.ac.uk/data_request/cif.

Low-pressure gas adsorption measurements were conducted using a Micromeritics ASAP 2020 volumetric gas adsorption instrument. The crystalline sample of $[Co_2(H_{0.67}bdt)_3]\cdot 20H_2O$ ($\mathbf{1}\cdot 20H_2O$) was transferred to preweighed analysis tubes, which were then capped with a transeal to prevent intrusion of atmospheric moisture during transfers and weighing. The sample was then evacuated under dynamic vacuum at 120 °C at a heating rate of 0.1 °C min^{-1} until the outgas rate was less than 2 mTorr min^{-1}. The evacuated analysis tube containing a degassed sample **1** was then weighed to determine the mass of the sample (typically 100–175 mg). For all isotherms, warm and cold free space correction measurements were taken using ultra-high-purity helium gas. The H_2 and N_2 isotherms at 77 K were measured in liquid nitrogen baths using UHP-grade gas sources.

Received: October 1, 2008
Revised: December 12, 2008
Published online: February 6, 2009

Keywords: cobalt · hydrothermal synthesis · magnetic properties · organic–inorganic hybrid composites

[1] S. Kitagawa, R. Kitaura, S. Noro, *Angew. Chem.* **2004**, *116*, 2388 – 2430; *Angew. Chem. Int. Ed.* **2004**, *43*, 2334 – 2375, and references therein.
[2] B. Chen, S. Ma, E. J. Hurtado, E. Lobkovsky, C. Liang, H. Zhu, S. Dai, *Inorg. Chem.* **2007**, *46*, 8705 – 8709, and references therein.
[3] D. J. Collins, H.-C. Zhou, *J. Mater. Chem.* **2007**, *17*, 3154 – 3160.
[4] M. Dinca, W. S. Han, Y. Liu, A. Dailey, C. M. Brown, J. R. Long, *Angew. Chem.* **2007**, *119*, 1441 – 1444; *Angew. Chem. Int. Ed.* **2007**, *46*, 1419 – 1422.
[5] J. L. C. Rowsell, O. M. Yaghi, *Angew. Chem.* **2005**, *117*, 4748 – 4758; *Angew. Chem. Int. Ed.* **2005**, *44*, 4670 – 4679.
[6] H. L. Ngo, W. B. Lin, *Top. Catal.* **2005**, *34*, 85 – 92.
[7] C. Janiak, *Dalton Trans.* **2003**, 2781 – 2804, and references therein.
[8] "Hybrid organic-inorganic electronics": D. B. Mitzi in *Functional Hybrid Materials* (Eds.: P. Gomez-Romero, C. Sanchez), Wiley-VCH, Weinheim, **2004**, pp. 347 – 386.
[9] G. Férey, *Chem. Soc. Rev.* **2008**, *37*, 191 – 214.
[10] S. Kitagawa, S. Noro, *Compr. Coord. Chem. II* **2004**, *7*, 231 – 261.
[11] S. L. James, *Chem. Soc. Rev.* **2003**, *32*, 276 – 288.
[12] M. H. Klingele, S. Brooker, *Coord. Chem. Rev.* **2003**, *241*, 119 – 132.
[13] U. Beckmann, S. Brooker, *Coord. Chem. Rev.* **2003**, *245*, 17 – 19.
[14] J. G. Haasnoot, *Coord. Chem. Rev.* **2000**, *200–202*, 131 – 185.
[15] H. Hayashi, A. P. Côté, H. Furukawa, M. O'Keefe, O. M. Yaghi, *Nat. Mater.* **2007**, *6*, 501 – 506.
[16] M. Dinca, A. F. Yu, J. R. Long, *J. Am. Chem. Soc.* **2006**, *128*, 8904 – 8913.
[17] J. Tao, Z.-J. Ma, R.-B. Huang, L.-S Zheng, *Inorg. Chem.* **2004**, *43*, 6133 – 6135.
[18] W. Ouellette, M. H. Yu, C. J. O'Connor, D. Hagrman, J. Zubieta, *Angew. Chem.* **2006**, *118*, 3577 – 3580; *Angew. Chem. Int. Ed.* **2006**, *45*, 3497 – 3500.
[19] W. Ouellette, J. R. Galán-Mascarós, K. R. Dunbar, J. Zubieta, *Inorg. Chem.* **2006**, *45*, 1909 – 1911.
[20] W. Ouellette, A. V. Prosvirin, V. Chieffo, K. R. Dunbar, B. Hudson, J. Zubieta, *Inorg. Chem.* **2006**, *45*, 9346 – 9366.
[21] W. Ouellette, B. S. Hudson, J. Zubieta, *Inorg. Chem.* **2007**, *46*, 4887 – 4904.
[22] W. Ouellette, A. V. Prosvirin, J. Valeich, K. R. Dunbar, J. Zubieta, *Inorg. Chem.* **2007**, *46*, 9067 – 9082.
[23] "Solid-state methods: hydrothermal": J. Zubieta, *Compr. Coord. Chem. II* **2003**, *1*, 667 – 709.
[24] $\mathbf{1}\cdot 20H_2O$: $C_3H_{6.5}Co_{0.25}N_3O_{2.5}$, $M_r = 139.34$, orthorhombic, *Cmmm*, $a = 7.5320(6)$, $b = 26.296(2)$, $c = 12.522(1)$ Å, $V = 2480.1(3)$ Å^3, $Z = 16$, $\rho_{calcd} = 1.493\ g\,cm^{-3}$, $R1 = 0.0355$, $wR2 = 0.0881$.
[25] A. Michalowicz, J. Moscovici, B. Ducourant, D. Cracco, O. Kahn, *Chem. Mater.* **1995**, *7*, 1833 – 1842.
[26] M. E. Fisher, *Am. J. Phys.* **1964**, *32*, 343 – 346.
[27] K. S. Cole, R. H. Cole, *J. Chem. Phys.* **1941**, *9*, 341 – 351.
[28] A. Caneschi, D. Gatteschi, N. Lalioti, C. Sangregorio, R. Sessoli, G. Venturi, A. Vindigni, A. Rettori, M. G. Pini, M. A. Novak, *Angew. Chem.* **2001**, *113*, 1810 – 1813; *Angew. Chem. Int. Ed.* **2001**, *40*, 1760 – 1763.
[29] X.-J. Li, X.-Y. Wang, S. Gao, R. Cao, *Inorg. Chem.* **2006**, *45*, 1508 – 1516.
[30] H. S. Yoo, J. I. Kim, N. Yang, E. K. Koh, J.-G. Park, C. S. Hong, *Inorg. Chem.* **2007**, *46*, 9054 – 9056.
[31] X.-M. Zhang, Z.-M. Hao, W.-X. Zhang, X.-M. Chen, *Angew. Chem.* **2007**, *119*, 3526 – 3529; *Angew. Chem. Int. Ed.* **2007**, *46*, 3456 – 3459.
[32] Z.-M. Sun, A. V. Prosvirin, H.-H. Zhao, J.-G. Mao, K. R. Dunbar, *J. Appl. Phys.* **2005**, *97*, 10B305.
[33] A. V. Palii, S. M. Ostrovsky, S. I. Klokishner, O. S. Reu, A.-M. Sun, A. V. Prosvirin, H.-H. Zhao, J.-G. Mao, K. R. Dunbar, *J. Phys. Chem. A* **2006**, *110*, 14003 – 14012.
[34] O. Kahn, J. Larionova, J. V. Yakhmi, *Chem. Eur. J.* **1999**, *5*, 3443 – 3449.
[35] G. J. Halder, C. J. Kepert, B. Moubaraki, K. S. Murray, J. D. Cashion, *Science* **2002**, *298*, 1762 – 1765.
[36] N. Yanai, W. Kaneko, K. Yoneda, M. Ohba, S. Kitagawa, *J. Am. Chem. Soc.* **2007**, *129*, 3496 – 3497.
[37] N. Lopez, H. Zhao, A. V. Prosvirin, A. Chouai, K. R. Dunbar, *Chem. Commun.* **2007**, 4611 – 4613.
[38] G. Férey, *Nat. Mater.* **2003**, *2*, 136 – 137.
[39] J. Tao, M.-J. Ma, R.-B. Huang, L.-S. Zheng, *Inorg. Chem.* **2004**, *43*, 6133 – 6138.
[40] a) Bruker: SMART, SAINT, SHELXTL, and SADABS. Bruker AXS Inc., Madison, Wisconsin, USA, **2002**; b) *International Tables for Crystallography*, International Union of Crystallography, *Vol. A*, 4th ed. (Ed.: T. Hahn), Kluwer Academic Publishers, Dordrecht, **1995**; c) A. L. Spek PLATON, A Multipurpose Crystallographic Tool, Utrecht University, Utrecht, The Netherlands, **2008**.
[41] A. L. Spek, *J. Appl. Crystallogr.* **2003**, *36*, 7 – 13.

